IEEE Access
Multidisciplinary | Rapid Review | Open Access Journal

Received January 24, 2021, accepted February 8, 2021, date of publication February 22, 2021, date of current version June 7, 2021.

Digital Object Identifier 10.1109/ACCESS.2021.3060773

Thermodynamic Analysis of a Novel Self-Air-Cooling Reciprocating Compressor

XIAOHUI GAO AND YONGGUANG LIU
School of Automation Science and Electrical Engineering, Beihang University, Beijing 100191, China
Corresponding author: Yongguang Liu (lyg@buaa.edu.cn)

This work was supported in part by the China Postdoctoral Science Foundation under Grant 2018M631299, and in part by the National Natural Science Foundation of China under Grant 11272026.

ABSTRACT A novel self-air-cooling reciprocating compressor (SACRC) is proposed, which can cool itself when it is working without adding any auxiliary equipment. The suction and discharge valve model are established considering thermodynamic and kinematics properties. The thermodynamic models of compressor and cooling system are respectively established considering their compressibility and heat exchange. The model of SACRC is finally achieved on the basis of building its energy network and it is verified by good curve-fitting between simulation and experiment at different conditions, which improves the compressor thermodynamic model theory. The results of characteristic analysis and comparative research show that the cooling system can obviously reduce the cylinder temperature and improve the volumetric efficiency, which makes it possible for compressor to realize high pressure and microminiaturization.

INDEX TERMS Thermodynamic model, self-air-cooling, compressor, characteristic analysis, comparative research.

I. INTRODUCTION

Reciprocating compressor, as a common equipment in industry, plays a huge role because of its high pressure, compact structure and clean energy [1], [2]. Due to the large amount of heat generated in the compression process, the efficiency of high pressure reciprocating compressor without cooling system is only around 20%, which is quite low compared with electrical or mechanical efficiency [3]. As an efficient cooling method, the liquid-cool [4]–[6] and air-cool [7], [8] are widely applied to cool the cylinder or inter-stage gas, which can even achieve isothermal compression. But they usually need additional auxiliary equipment and consume even more energy than compression. Through improving the structure, the liquid piston [9] and finned [2] reciprocating compressor are put forward and applied in the low-pressure situation. This paper proposes a self-air-cooling reciprocating compressor (SACRC), which can cool the cylinder through airflow produced by itself without any auxiliary equipment. It does not need additional energy consumption and the volume and weight may be reduced. So, the thermodynamic analysis becomes the key to further improve its performance.

The associate editor coordinating the review of this manuscript and approving it for publication was Dominik Strzalka.

The thermodynamic model of reciprocating compressor is firstly established by Costagliola and Great Neck in 1950 [10]. However, the research process was relatively slow due to underdeveloped computer technology. Since 1972, the international conference on compressor engineering held by Purdue University published a lot of high-level papers, which became the research direction of compressor industry. At present, the modeling methods of reciprocating compressor mainly consist of the polytropic equation based on Van der Wals [11], [12], the first thermodynamic law [13], computational fluid dynamics model [14], [15] and the second theorem of thermal dynamics [16], [17].

The mathematical model of compressor based on the first thermodynamic law can intuitively describe the thermodynamic process in the sight of energy conservation. Soedel W and Hamilton J.F firstly built the thermodynamic model of the reciprocating compressor [18], [19]. Prakash R and Todescat added the heat transfer between gas and cylinder into this model [20], [21]. Giovanni studied the performance and stability of the compressor heat transfer [22]. Wang J built the thermodynamic model including of gas leakage and unstable heat transfer, which regarded the compressor as a variable mass system [23]. Mahmood and Amir built the thermodynamic model of real gas and studied the effects of angular velocity, pressure ratio and clearance on compressor

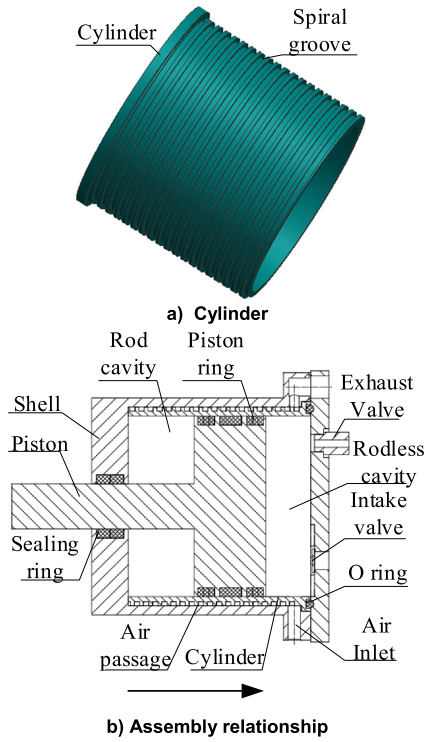

FIGURE 1. Mechanism of SACRC.

efficiency [24], [25]. Although the simulation data could agree well with the experiment, they are established based on their own special conditions. As the cooling system is integrated into the compressor, the thermodynamic model of SACRC is far more complex than traditional reciprocating compressor (TRC) without cooling system. In order to study the cooling characteristics of SACRC, the thermodynamic model of SACRC is achieved through establishing the model of each component and their energy transfer network and it is verified by experiment under different conditions. On this basis, its thermodynamic characteristic is studied through analysis and comparison.

II. WORKING PRINCIPLE OF SACRC

The mechanism of SACRC is shown in Fig.1. The cooling system is composed of air passage and rod cavity. The spiral groove is machined on the cylinder outer wall (Fig.1-a), which forms air passage with shell (Figure 1-b). The rod cavity is closed by sealing ring, which is connected to the air passage (Fig.1-b). When the piston moves along the direction of arrow (Fig.1-b), the gas in rodless cavity is compressed and exhausted through discharge valve and the air flows into rod cavity through spiral groove and air inlet. The compressed gas may be air, natural gas or nitrogen, while the air in rod cavity is from atmosphere. As the equivalent diameter of rod cavity is much larger than spiral groove, the air is always turbulent in passage, which increases the forced convection heat transfer coefficient. The cylinder is heated by compressed gas and its temperature is always higher than the air in spiral groove. So, the cylinder is cooled and the heat of the compressed gas

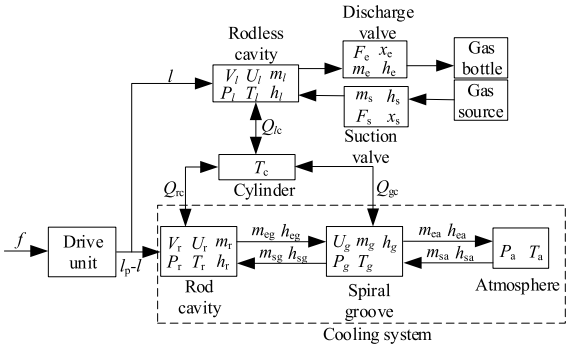

FIGURE 2. Energy transfer network.

is dissipated quickly, which can increase the mass flow rate of the exhaust and improve the compressor's efficiency. When the piston moves along the opposite direction of arrow, the air in the rod cavity is discharged through spiral groove and it can also cool the cylinder, which can improve suction quality. The rod cavity is fully applied to cool the cylinder and the rodless cavity is applied to output high pressure gas. So, the SACRC can realize self-cooling and improve its efficiency.

III. MATHEMATICAL MODEL

The SACRC is mainly composed of drive unit, rodless cavity, rod cavity, spiral groove and cylinder. The energy transfer network among components is shown in Fig.2. The P, T, U, V, h and m respectively are pressure, temperature, internal energy, volume, enthalpy and mass. The subscripts l, r, g and a respectively are rodless cavity, rod cavity, spiral groove and atmosphere. The relationships among U, h, T are as follows [26].

$$U = mc_vT \tag{1}$$

$$h = c_pT \tag{2}$$

$$c_p = (28.15 + 1.967 \times 10^{-3} \times T + 4.801 \times 10^{-6} \times T^2 - 1.966 \times 10^{-9} \times T^3)/M_0 \tag{3}$$

$$c_v = c_p - r_0 \tag{4}$$

where c_p is the constant pressure specific heat, c_v is the constant volume specific heat, r_0 is the gas constant.

The mathematical models of each component are respectively established and the system model can be achieved according to the mass and energy transmission and conversion among them.

A. DRIVE UNIT

The piston moves back and forth along sine curve driven by crankshaft or swash plate. The stroke of piston l is

$$l = \frac{l_p}{2} + \frac{l_p}{2}\sin(2\pi ft) \tag{5}$$

where l_p and f respectively are the motion amplitude and frequency of piston.

When SACRC works, the volume of the rod and rodless cavity respectively are V_r and V_l. The relationships among

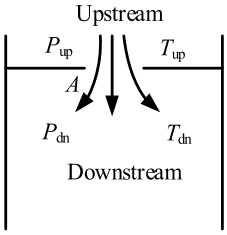

FIGURE 3. Mass flow parameters.

P, V, T and m satisfy the differential equation of gas state (Eq.8).

$$V_l = l\pi d^2/4 + V_0 \tag{6}$$

$$V_r = \pi(l_p - l)(d^2 - d_r^2)/4 + V_{r0} \tag{7}$$

$$\frac{dP}{dt} = \frac{1}{V}(r_0 T\frac{dm}{dt} + r_0 m\frac{dT}{dt} - P\frac{dV}{dt}) \tag{8}$$

where V_0 is the clearance volume of rodless cylinder, d is inner diameter of cylinder, V_{r0} is the clearance volume of rod cylinder, d_r is piston rod diameter.

B. CHECK VALVE

The check valve is used for the suction and discharge valves to ensure one-way flow of gas. When the gas pressure is higher than the opening pressure of valve, the valve core moves under the action of aerodynamic force. The gas mass flow is determined by the opening of valve core. Therefore, the model should include differential equations of gas flow rate and valve core spool movement

When the check valve is open, the gas begins to flow with varying thermodynamic properties. The following assumptions should be made.

1) When the gas flows through valve port, its thermodynamic parameters remain uniform in any transient procedures.

2) The damping force and pressure pulsation of gas are both ignored.

3) The valve port is regarded as a small hole in the effective flow cross section.

The mass flow $\dot{m}$ through valve is shown in Eq.9 [27].

$$\dot{m} = AC_m C_q \frac{P_{up}}{\sqrt{T_{up}}} \tag{9}$$

where A is the effective orifice area of valve, C_m is the flow parameter, C_q is the flow coefficient, P_{up} is the upstream pressure and T_{up} is the upstream temperature (Fig.3).

When the suction valve opens, the gas source is upstream and rodless cavity is downstream. When the discharge valve opens, the rodless cavity is upstream and the gas bottle is downstream.

The reed and poppet valve are respectively regarded as suction and discharge valve. When their openings respectively are x_s and x_e, the effective orifice area A_s and A_e are shown in Eq.10 [28] and Eq.11 [27].

$$A_s = \pi d_s x_s \tag{10}$$

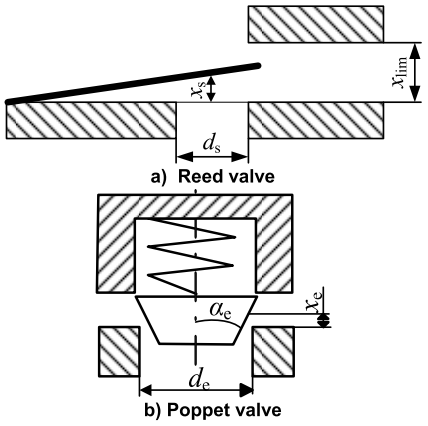

FIGURE 4. Valve parameters.

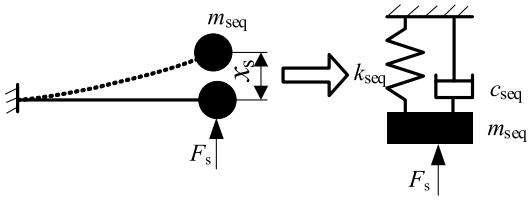

FIGURE 5. Equivalent model of reed valve.

$$A_e = \pi x_e \sin\alpha_e(d_e - x_e \sin\alpha_e \cos\alpha_e) \tag{11}$$

The valve parameters are shown in Fig.4.

The mass flow parameter C_m can be written as follows [27].

$$C_m = \begin{cases} \sqrt{\dfrac{2\gamma}{r_0(\gamma-1)}}\sqrt{(\dfrac{P_{dn}}{P_{up}})^{\frac{2}{\gamma}} - (\dfrac{P_{dn}}{P_{up}})^{\frac{\gamma+1}{\gamma}}} \\ \quad \dfrac{P_{dn}}{P_{up}} > P_{cr} \text{ (Subsonic)} \\ \sqrt{\dfrac{2\gamma}{r_0(\gamma+1)}}(\dfrac{2}{\gamma+1})^{\frac{1}{(\gamma-1)}} \\ \quad \dfrac{P_{dn}}{P_{up}} \le P_{cr} \text{ (Sonic)} \end{cases} \tag{12}$$

where $\gamma = c_p/c_v$ is the specific heat ratio, P_{cr} is the critical pressure ratio, P_{dn} is the downstream pressure (Fig.3).

The reed valve is a single freedom system with one end fixed and one end free. It can be equivalent to a spring-mass-damper system of single freedom (Fig.5). The poppet valve is also a single freedom. So, the motion differential equation is

$$m_{eq}\ddot{x} + c_{eq}\dot{x} + k_{eq}x = F - F_0 \tag{13}$$

where m_{eq}, c_{eq}, k_{eq}, F and F_0 respectively are equivalent mass, damping coefficient, stiffness, aerodynamic force and pre-pressure of valve.

When the reed valve opens, the deflection is inconformity in different positions. The distributed mass system is simplified as a single degree of freedom system based on the energy

conservation [29].

$$m_{\mathrm{seq}} = \frac{33}{140}\rho_{\mathrm{s}} b_{\mathrm{s}} \delta_{\mathrm{s}} l_{\mathrm{s}} \tag{14}$$

where $\rho_{\mathrm{s}}, b_{\mathrm{s}}, \delta_{\mathrm{s}}, l_{\mathrm{s}}$ respectively are the density, width, thickness and length of reed valve.

The reed valve is regarded as a single degree of freedom cantilever beam. The equivalent stiffness is shown in Eq.15 [29].

$$k_{\mathrm{seq}} = \frac{E_{\mathrm{s}} b_{\mathrm{s}} \delta_{\mathrm{s}}^3}{l_{\mathrm{s}}^3} \tag{15}$$

where E_{s} is the elasticity modulus of reed valve.

The aerodynamic force acting on the valve core F is

$$F = A(P_{\mathrm{up}} - P_{\mathrm{dn}}) \tag{16}$$

The rod and rodless cavity are both variable volume and the gases in them satisfy the first law of thermodynamics, mass conservation equation and gas state equation.

According to the first law of thermodynamics, the gas thermodynamic energy conservation equation is shown in Eq.17.

$$\frac{\mathrm{d}U}{\mathrm{d}t} = \frac{\mathrm{d}Q}{\mathrm{d}t} - \frac{\mathrm{d}W}{\mathrm{d}t} + \ddot{m}_{\mathrm{s}} h_{\mathrm{s}} - \dot{m}_{\mathrm{e}} h_{\mathrm{e}} \tag{17}$$

$$\frac{\mathrm{d}W}{\mathrm{d}t} = P\frac{\mathrm{d}V}{\mathrm{d}t} \tag{18}$$

where Q is the heat exchange between gas and cylinder, W is the work of piston, m_s, h_s respectively are the mass and enthalpy of the gas entering cavity, m_e, h_e respectively are the mass and enthalpy of the gas discharged from cavity.

$$Q = HS\Delta T \tag{19}$$

where H, S and ΔT respectively are the coefficient of convection heat transfer, heat convection area and temperature difference between cylinder and gas.

The convection heat transfer coefficient between cylinder and gas in rod and rodless cavity is shown in Eq.20 [24].

$$H = 3.26 d^{-0.2} P^{0.8} T^{-0.55} (2.28\overline{v})^{0.8} \tag{20}$$

where $\overline{v}$ is the average speed of piston.

$$\overline{v} = 0.637 \times 2\pi f l \tag{21}$$

C. SPIRAL GROOVE

When the piston moves, the air can flow into or out of the rod cavity through spiral groove. The mass and energy exchange exist between spiral groove and rod cavity, spiral groove and atmosphere. As the equivalent hydraulic diameter of spiral groove is far less than rod cavity, the flow rate of air in spiral groove is high and the flow resistance isn't ignored. So, the spiral groove can be equal to a chamber with compressibility and heat exchange.

The air in spiral groove meets the first law of thermodynamics, mass conservation equation and gas state equation. As the volume is fixed, $P\frac{\mathrm{d}V}{\mathrm{d}t}$ is 0.

$$\frac{\mathrm{d}U_{\mathrm{g}}}{\mathrm{d}t} = \frac{\mathrm{d}Q_{\mathrm{gc}}}{\mathrm{d}t} + \ddot{m}_{\mathrm{sg}} h_{\mathrm{sg}} - \dot{m}_{\mathrm{eg}} h_{\mathrm{eg}} \tag{22}$$

where Q_{gc} is the heat exchange between cylinder and air in spiral groove, m_{sg} and h_{sg} are the mass and enthalpy of the air entering spiral groove from atmosphere and rod cavity, m_{eg} and h_{eg} are the mass and enthalpy of the air discharged from spiral groove.

$$Q_{\mathrm{gc}} = c_g H_{\mathrm{gc}} \pi d_g l_g (T_{\mathrm{c}} - T_g) \tag{23}$$

where H_{gc} is the convective exchange coefficient between cylinder and air in spiral groove, d_g, l_g respectively are the equivalent diameter and length of spiral groove.

The helical tube correction factor c_g is [30]

$$c_{\mathrm{g}} = 1 + 3.54\frac{d_g}{d_{\mathrm{c}}} \tag{24}$$

$$H_{\mathrm{gc}} = \frac{Nu\lambda_g}{\mathrm{d}_g} \tag{25}$$

where λ_{g}, Nu are respectively the heat conductivity coefficient and Nusselt number of the air in the spiral groove.

When the air pressure is between 100Pa and 1Mpa, λ_{s} is only related to temperature [26].

$$\lambda_{\mathrm{g}} = \lambda_0 (\frac{T_{\mathrm{g}}}{273.15})^{0.8} \tag{26}$$

where $\lambda_0 = 2.44 \times 10^{-2}$W/m.K is the air heat conductivity coefficient at 273.15K.

When the air is respectively in laminar flow, transition and turbulence, Nu are shown in Eq.27 [26].

$$\begin{cases} Nu_{\mathrm{lam}} = 1.86(\mathrm{Re} \bullet \mathrm{Pr})^2 (\frac{\mu_0}{\mu_{\mathrm{g}}})^{0.14} \\ \qquad \mathrm{Re} < 80\frac{d_g}{\Delta} (\text{laminar flow}) \\ \frac{1}{2}[(1 - k_{N\mathrm{u}})Nu_{\mathrm{lam}} + (1 + k_{N\mathrm{u}})Nu_{\mathrm{tur}}] \\ \qquad 80\frac{d_g}{\Delta} < \mathrm{Re} < 4160(\frac{d_g}{\Delta})^{0.85} (\text{transition}) \\ Nu_{\mathrm{tur}} = 0.027 Re^{0.8} \mathrm{Pr}^{1/3} (\frac{\mu_0}{\mu_{\mathrm{g}}})^{0.14} \\ \qquad \mathrm{Re} > 4160(\frac{d_g}{\Delta})^{0.85} (\text{turbulence}) \end{cases} \tag{27}$$

$$k_{N\mathrm{u}} = \tanh(8\frac{\mathrm{Re} - 80\frac{d_{\mathrm{g}}}{\Delta}}{4160(\frac{d_{\mathrm{g}}}{\Delta})^{0.85} - 80\frac{d_{\mathrm{g}}}{\Delta}} - 4) \tag{28}$$

where μ_{g} is the air dynamic viscosity, $\Delta = 45\ \mu m$ is absolute roughness of the spiral groove, Re is Reynolds number, Pr is Prandtl number.

The mass flow can also be calculated by Eq.9. Considering the friction in the spiral groove, the equivalent flow coefficient is

$$C_{qg} = \sqrt{\frac{d_g}{l_g f_g}} \tag{29}$$

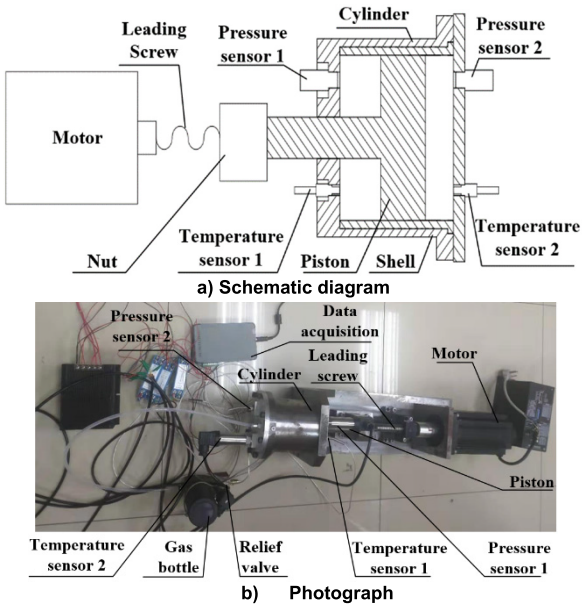

FIGURE 6. SACRC testbed.

The f_g depends on the Reynolds number Re [26].

$$\begin{cases} f_g = \dfrac{64}{\mathrm{Re}} \\ \quad \mathrm{Re} < 80\dfrac{d_g}{\Delta}(\text{laminar flow}) \\ \dfrac{1}{\sqrt{f_g}} = -2\lg(\dfrac{\Delta}{3.7d_g} + \dfrac{2.51}{Re\sqrt{f_g}}) \\ \quad 80\dfrac{d_s}{\Delta} < \mathrm{Re} < 4160(\dfrac{d_g}{\Delta})^{0.85}(\text{transition}) \\ f_g = \dfrac{1}{[2\lg(\frac{d_g}{2\Delta}) + 1.74]^2} \\ \quad \mathrm{Re} > 4160(\dfrac{d_g}{\Delta})^{0.85}(\text{turbulence}) \end{cases} \tag{30}$$

$$\mathrm{Re} = \frac{4\left|\frac{dm}{dt}\right|}{\pi\mu d_s} \tag{31}$$

D. CYLINDER

The cylinder temperature is changed by heat exchange.

$$Q_{lc} + Q_{rc} + Q_{gc} = C_c m_c \Delta T_c \tag{32}$$

where $C_c = 480$ J/kg.K is the average specific heat capacity of cylinder when its material is steel, m_c is the cylinder mass, ΔT_c is the cylinder temperature change.

IV. EXPERIMENT RESEARCH

A. EXPERIMENT TESTBED

The SACRC testbed is shown in Fig.6, which is composed of controller, motor, leading screw, piston, cylinder, pressure sensor, temperature sensor, relief valve and data acquisition. The motor drives the piston along the sine through leading screw. Smaq USB-3110, as a data acquisition, is used to collect pressure and temperature by sensor and its sampling period is 10ms. The pressure sensor1, temperature sensor1, pressure sensor2 and temperature sensor2 are respectively applied to test the pressure and temperature of gas in the rod and rodless cavity (Fig.6-a). The parameters of sensors are shown in Table.1. The piston motion frequency can be adjusted through controlling the speed of motor. The output pressure is regulated by relief valve.

TABLE 1. parameters of SENSOR.

Sensor	Series	Manufacturers	Range	Accuracy
Pressure sensor1	HH-319	Huahai	-0.1~2Mpa	0.1%F.s
Pressure sensor2	HH-319	Huahai	-0.1~2Mpa	0.1%F.s
Temperature sensor1	AE-WB	Aier	-50~150℃	0.1%F.s
Temperature sensor1	AE-WB	Aier	-50~150℃	0.1%F.s

The speed of motor can be adjusted by controller. The lead of leading screw is 5mm and the stroke of piston is 60mm. When the frequency of the compressor is 0.5Hz, 1Hz and 2Hz, the motor speed can be set 720r/min, 1440r/min and 2880r/min. The relief valve is used to adjust the pressure ratios. When pressure ratios respectively are 3, 6 and 9, the discharge pressure of relief valve is set 3bar, 6bar and 9bar.

B. MODEL VERIFICATION

When the compressor works at 0.5Hz for 50 seconds and the pressure ratios respectively are 3, 6 and 9, the gas performances of rod and rodless cavity at the last cycle are shown in Fig.7. The pressure curves of simulation fit very well with the experiment at different pressure ratios. As the leakage is ignored, the pressure and temperature of gas in experiment are always lower than simulation. As the response of temperature sensor is low, the test value is always lower than the real value. So, the fitting of temperature curve is worse than pressure. When the pressure difference of valve on both sides is higher than opening pressure, the rodless cavity begins to inhale or discharge. The check valve mainly affects the minimum and maximum pressure of gas in the rodless cavity especially at a larger pressure ratio (Fig.7-a) and the gas temperature also varies greatly in the suction and discharge (Fig.7-b). Therefore, the check valve model has an important impact on the thermodynamic characteristic of compressor especially at high pressure ratio. The temperature and pressure of air in the rod cavity don't fluctuate much in one period (Fig.7-c, Fig.7-d). Due to the more heat can be produced at high pressure ratio, it is transferred to the air in spiral groove and rod cavity (Fig.7-d).

When the compressor works at pressure ratio 6 for 30 cycles and the driving frequencies respectively are 0.5Hz, 1Hz and 2Hz, the performance of gas for the 30th cycle in rodless and rod cavity are shown in Figure 8. The pressure and temperature curves of simulation fit very well with the experiment at different frequencies. As the velocity and

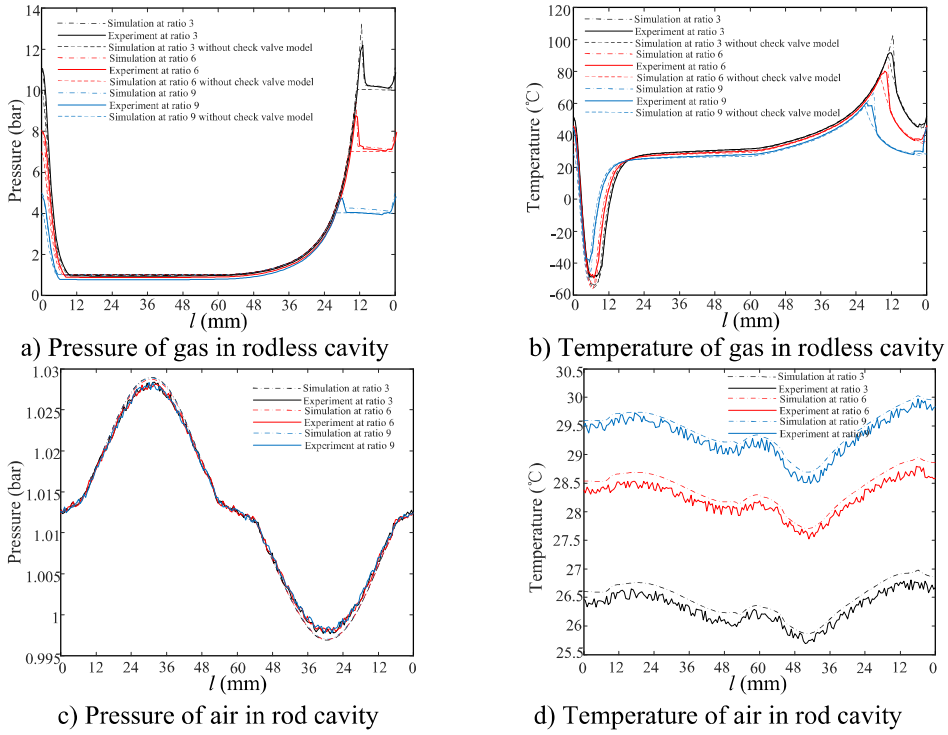

FIGURE 7. Gas performance at different pressure ratios.

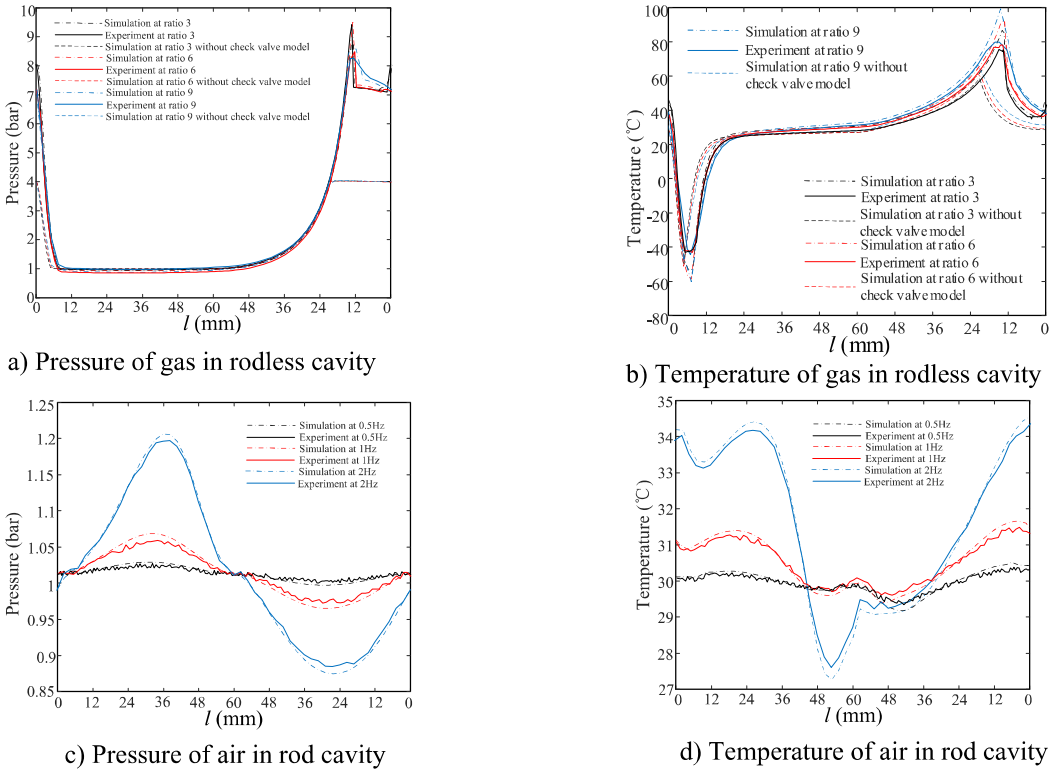

FIGURE 8. Gas performance at different frequencies.

flow resistance of gas are related to frequency, the check valve increases pressure and temperature especially at high frequency (Fig.8-a, Fig.8-b). When the compressor works at high frequency, the more heat is produced and temperature

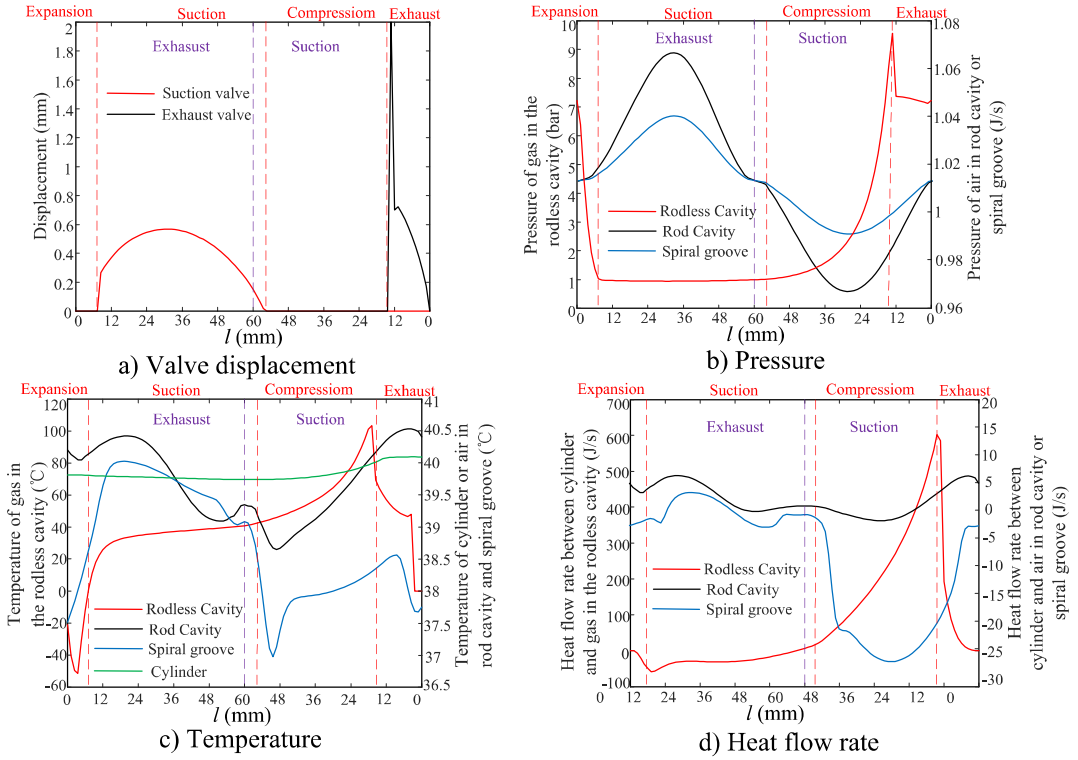

FIGURE 9. SACRC's characteristics in one cycle.

difference in one cycle is larger (Fig.8-b). Although the movement performance of valve core is affected at different frequencies, once the pressure ratio is determined, the pressure and temperature change little in a cycle. As the air flows into or out of rod cavity through the slender spiral groove, the pressure of rod cavity is closely related to the frequency. When the compressor works at high frequency, the air in spiral groove flows faster. So, the air pressure and temperature difference in rod cavity are both larger in one cycle because of higher flow resistance and heat transfer (Fig.8-c, Fig.8-d).

V. CHARACTERISTIC ANALYSIS

According to the working principle of the SACRC, the mathematical model is established and its differential equations are solved by Runge-Kutta method. When the stroke of piston is 60mm, the transient characteristics in one cycle are achieved (Fig.9). The rodless cavity is used to compress gas and it goes through four stages of expansion, suction, compression and discharge in one cycle. The red broken lines in this figure are the boundaries between two stages. The rod cavity and spiral groove are used to cool the cylinder and there is no boundary between expansion and suction, compression and discharge. The dotted purple lines in the figure are the boundary between two stages.

The working process is described according to four stages of rodless cavity.

1) Gas characteristics of rodless cavity in expansion

The suction valve is closed (Fig.9-a). The pressure gradually decreases (Fig.9-b) and the temperature decreases first and then increases gradually (Fig.9-c). The expansion can consume heat and lower gas temperature. The heat flow rate from cylinder to gas gradually increases because the piston speeds up and the heat exchange coefficient increases (Fig.9-d). So, the heat absorbed from cylinder becomes gradually higher. When the amount of heat absorbed from cylinder is higher than consumed by expansion, the gas temperature starts to rise.

2) Gas characteristics of rodless cavity in suction

The opening of suction valve first increases and then decreases (Fig.9-a). Due to the inertia, the suction valve closes after reverse motion of piston. The pressure decreases first and then increases, but its change is little (Fig.9-b). Although the flow resistance is related to valve opening, it is not important at low flow. The temperature gradually increases, but its amplitude is not big. The heat flow rate is small (Fig.9-d). Because the temperature difference between gas and cylinder, pressure and flow rate of gas are all low.

3) Gas characteristics of cooling system in discharge

When the rodless cavity is in expansion and suction, the cooling system is in discharge. The pressure of air in rod cavity and spiral groove first increase and then decrease (Fig.9-b). The pressure is mainly related to the flow resistance that depends on the piston velocity. The air in rod cavity flows out through the spiral groove. So, the pressure of air in rod cavity is always higher than spiral groove (Fig.9-b). The temperature of air in rod cavity and spiral groove both fluctuate up and down around the cylinder (Fig.9-c), but its amplitude change of spiral groove is much larger than rod

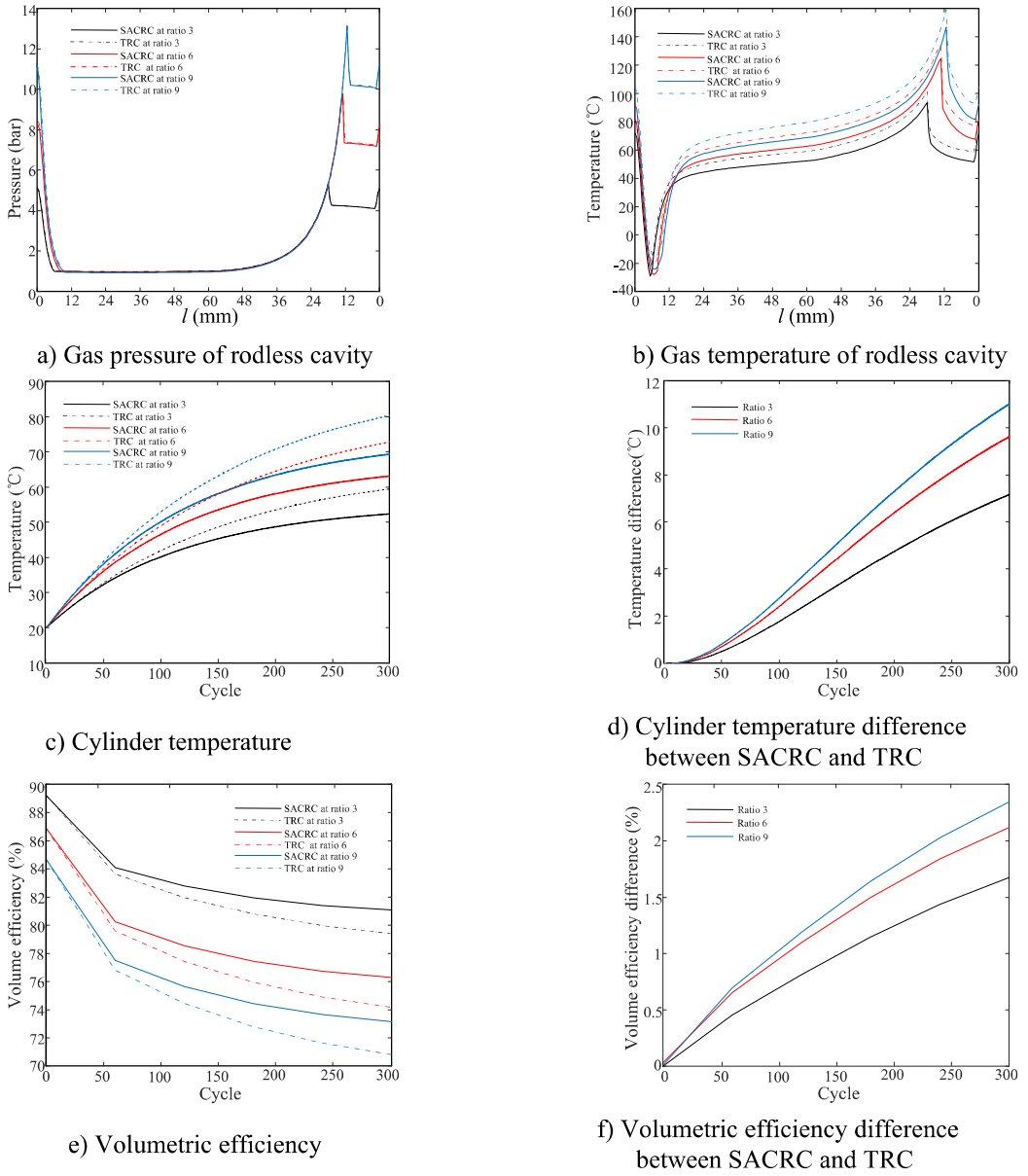

a) Gas pressure of rodless cavity

b) Gas temperature of rodless cavity

c) Cylinder temperature

d) Cylinder temperature difference between SACRC and TRC

e) Volumetric efficiency

f) Volumetric efficiency difference between SACRC and TRC

FIGURE 10. Performance of compressor at different pressure ratios.

cavity. This is because the heat exchange between cylinder and air in spiral groove is excellent. The air temperature of spiral groove is raised rapidly to near cylinder and the heated air is discharged (Fig.9-c), which is called discharge cooling.

4) Gas characteristics of rodless cavity in compression

The suction and discharge valve are both closed (Fig.9-a). The pressure increases rapidly (Fig.9-b) and the temperature increases fast first and then decreases (Fig.9-c). The heat generated by compression is transferred quickly to the cylinder (Fig.9-d), which increases the cylinder temperature (Fig.9-c). As the heat produced by compression is smaller than heat exchange at the end of the compression, the air temperature decreases (Fig.9-c).

5) Gas characteristics of rodless cavity in discharge

The discharge valve opens quickly and closes gradually (Fig.9-a). The high-pressure gas is discharged and its pressure and temperature quickly decrease (Fig.9-b, Fig.9-c). The heat flow rate quickly drops to zero (Fig.9-d).

6) Gas characteristics of cooling system in suction

When the rodless cavity is in compression and discharge, the cooling system is in suction. The pressure of air in spiral groove first decreases and then increases (Fig.9-b). The air flows into the rod cavity through the spiral groove. Although the air temperature of spiral groove fluctuates up and down (Fig.9-c), it is always lower than cylinder (Fig.9-c). The heat is quickly transferred to the air from the cylinder, which is called suction cooling.

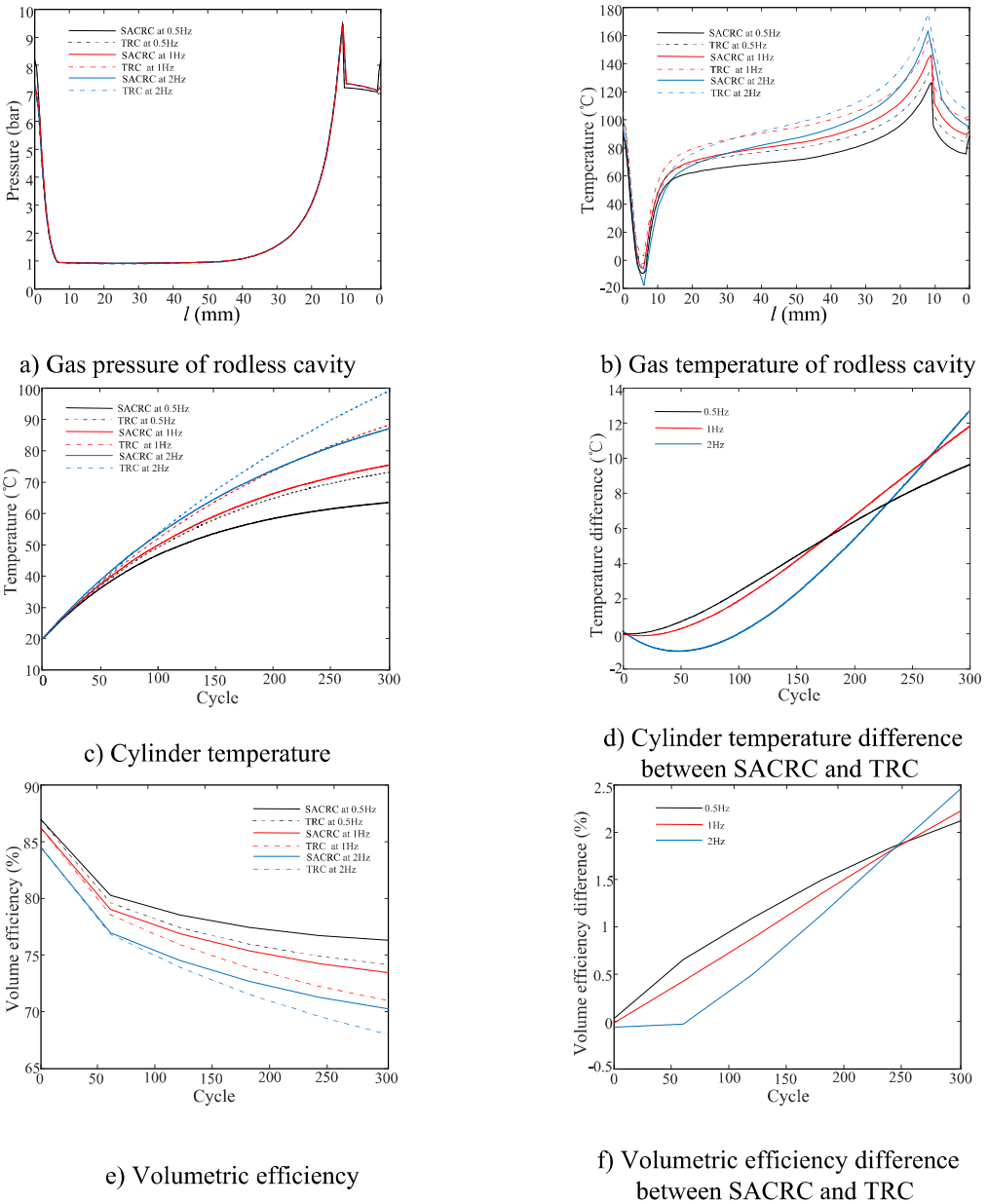

a) Gas pressure of rodless cavity

b) Gas temperature of rodless cavity

c) Cylinder temperature

d) Cylinder temperature difference between SACRC and TRC

e) Volumetric efficiency

f) Volumetric efficiency difference between SACRC and TRC

FIGURE 11. Performance of compressor at different frequencies.

Therefore, the cylinder can be cooled by suction and discharge cooling of spiral groove which exists in each cycle. This continuous cooling can reduce the rate of temperature rising of compressor and improve its efficiency.

VI. CONTRASTIVE RESEARCH BETWEEN TRC AND SACRC

The difference between the traditional TRC and SACRC is the cooling system, which is mainly applied to cool the cylinder. The performance of cooling system is studied by contrastive research between TRC and SACRC at different pressure ratios and frequencies.

The volumetric efficiency is applied to evaluate the performance of the compressor and it is calculated by Eq.33 [31].

$$\eta_v = \frac{m_{real}}{m_{ideal}} = \frac{m_{real}}{\rho_i V_c} \tag{33}$$

where m_{real} is mass through suction value per cycle, ρ_i is the suction gas density, V_c is the cylinder volume.

A. PRESSURE RATIO

When the compressor works at 0.5Hz for 300 cycles and the pressure ratios respectively are 3, 6 and 9, the performances of SACRC and TRC at the last cycle are shown in Figure 10. Although the gas pressure of rodless cavity in the SACRC is lower than that of TRC, their differences are all very small at different pressure ratios (Fig.10-a). The gas temperature of rodless cavity and cylinder increases significantly with the increase of pressure ratio (Fig.10-b, Fig.10-c). The gas temperature of SACRC is much lower than that of TRC. The cylinder temperature difference between SACRC and TRC increases with pressure ratio and cycle times (Fig.10-d).

So, the cooling effect is more obvious at high pressure ratio. With the increase of cycle times and pressure ratio, the volumetric efficiency of SACRC and TRC quickly drops (Fig.10-e). The volumetric efficiency of SACRC is always higher than that of TRC (Fig.10-e). The volumetric efficiency difference between SACRC and TRC increases with pressure ratio and the number of cycles (Fig.10-f). Therefore, the cooling system of SACRC can obviously reduce cylinder temperature and improve volumetric efficiency especially at high pressure ratio and long work hours.

B. FREQUENCY

When the compressor works at pressure ratio 6 for 300 cycles, the driving frequencies respectively are 0.5Hz, 1Hz and 2Hz, the performances of SACRC and TRC at the last cycle are shown in Fig.11. The change of gas pressure is not obvious (Fig.11-a). As the more heat is produced at high frequency, the gas temperature difference in one cycle increases significantly with the frequency (Fig.11-b) and the cylinder temperature increases larger (Fig.11-c). The cylinder temperature difference between SACRC and TRC is higher at high frequency and long work hours (Fig.11-d). So, the cooling effect is more obvious at high frequency. The volumetric efficiency quickly drops with frequency and it is always higher in the SACRC than TRC (Fig.11-e). The volumetric efficiency difference between SACRC and TRC is higher at high frequency and long work hours (Fig.11-f). Therefore, the cooling system of SACRC can obviously reduce cylinder temperature and improve volumetric efficiency especially at high frequency and long work hours.

VII. CONCLUSION

The following conclusions can be drawn through establishing thermodynamic model, experiment research, characteristic analysis and contrastive research.

1. The good fitting between simulation and experiment at different conditions proves this thermodynamic model.

2. The check valve model has an important impact on the thermodynamic characteristic in suction and discharge especially at high pressure ratio.

3. The cylinder can be cooled by suction and discharge of cooling system at per cycle.

4. The cooling system of SACRC can obviously reduce cylinder temperature and improve volumetric efficiency especially at high pressure ratio, high frequency and long work hours.

APPENDIX A
NOMENCLATURE

A	Area (m^2)
C	Specific heat capacity ($kJ(kg.K)^{-1}$)
c_v	Specific heat at constant volume ($kJ(kg.K)^{-1}$)
c_p	Specific heat at constant pressure ($kJ(kg.K)^{-1}$)
c_{eq}	Equivalent damping coefficient ($N.(m.s^{-1})^{-1}$)
C_m	Flow parameter
C_q	Flow coefficient
d	Diameter (m)
f	Motion frequency (Hz)
h	Enthalpy ($kJ.kg^{-1}$)
H	Convective exchange coefficient $J(m^2.K.s)^{-1}$
k_{eq}	Equivalent stiffness (N.m -1)
l	Length (m)
m	Mass (kg)
M_0	Gas molar mass.
P	Pressure (Pa)
Q	Heat exchange (J)
T	Temperature (K)
ΔT	Temperature change(K)
V	Working volume (m^3)
$\overline{v}$	Average velocity($m.s^{-1}$)
V_0	Clearance volume (m^3)
U	Internal energy (J)
ρ	Density($kg.m^{-3}$)
μ	Dynamic viscosity ($N.s(m^2)^{-1}$)

Subscript

a	air
c	cylinder
d	downstream
e	exhaust
l	rodless cavity
p	piston
r	rod cavity
s	suction
g	spiral groove
u	upstream

REFERENCES

[1] S. Jun, Y. S. Kang, and B. J. Lim, "Ported shroud design of a compressor for the hydrogen reciprocating engine of a high-altitude unmanned aerial vehicle," *J. Mech. Sci. Technol.*, vol. 33, no. 5, pp. 2113–2122, May 2019.

[2] M. Heidari, M. Mortazavi, and A. Rufer, "Design, modeling and experimental validation of a novel finned reciprocating compressor for isothermal compressed air energy storage applications," *Energy*, vol. 140, pp. 1252–1266, Dec. 2017.

[3] J. Tuhovcak, J. Hejcik, and M. Jicha, "Comparison of heat transfer models for reciprocating compressor," *Appl. Thermal Eng.*, vol. 103, pp. 607–615, Jun. 2016.

[4] B. Francesco, F. Giovanni, and B. Alberto, "Reciprocating compressor cylinder's cooling: A numerical approach using CFD with conjugate heat transfer," in *Proc. Pressure Vessels Piping Conf.*, 2014, pp. 1–10.

[5] G. Jia, M. Cai, W. Xu, and Y. Shi, "Energy conversion characteristics of reciprocating piston quasi-isothermal compression systems using water sprays," *Sci. China Technol. Sci.*, vol. 61, no. 2, pp. 285–298, Feb. 2018.

[6] Y. Deng, N. Miao, Y. Liu, X. Zhai, and D. Wu, "Investigation on cooling efficiency of a 3D-printed integrated inter cooler applicable to a miniature multi-stage compressor," *Int. J. Refrig.*, vol. 100, pp. 295–306, Apr. 2019.

[7] Y. F. Zhu, "Development of reciprocating air-cool oilless compressors series product," *Adv. Mater. Res.*, vols. 201–203, pp. 1429–1432, Feb. 2011.

[8] Y. Zhao, J. Feng, and Q. Zhou, "Blade fracture analysis of a motor cooling fan in a high-speed reciprocating compressor package," *Eng. Failure Anal.*, vol. 89, pp. 88–89, Dec. 2018.

[9] J. D. Van De Ven and P. Y. Li, "Liquid piston gas compression," *Appl. Energy*, vol. 86, no. 10, pp. 2183–2191, Oct. 2009.

[10] O. Costagliola, M. Great, and N. Neck, "The theory of spring-loaded valves for reciprocting compressors," *J. Appl. Mech.*, vol. 17, no. 4, pp. 415–420,1950.
[11] E. Ng, A. Tramschek, and J. MacLaren, "Computer simulation of a reciprocating compressor using a real gas equation of state," in *Proc. Int. Compressor Eng. Conf.* West Lafayette, IN, USA: Purdue Univ., 1980, pp. 33–42.
[12] T. Dutra and C. J. Deschamps, "Experimental characterization of heat transfer in the components of a small hermetic reciprocating compressor," *Appl. Thermal Eng.*, vol. 58, nos. 1–2, pp. 499–510, Sep. 2013.
[13] J. Brablik, "Some practical application of modern compressor valve technology gas pulsations as factor affecting operation of automation valves in reciprocating compressors," in *Proc. Int. Compressor Eng. Conf.* West Lafayette, IN, USA: Purdue Univ., 1972, pp. 188–195.
[14] C. Willich, C. N. Markides, and A. J. White, "An investigation of heat transfer losses in reciprocating devices," *Appl. Thermal Eng.*, vol. 111, pp. 903–913, Jan. 2017.
[15] O. Yasar and O. Kocas, "Computational modeling of hermetic reciprocating compressors," *Int. J. High Perform. Comput. Appl.*, vol. 21, no. 1, pp. 30–41, 2007.
[16] A. Morriesen and C. J. Deschamps, "Experimental investigation of transient fluid flow and superheating in the suction chamber of a refrigeration reciprocating compressor," *Appl. Thermal Eng.*, vol. 41, pp. 61–70, Aug. 2012.
[17] W. Li, "Simplified steady-state modeling for variable speed compressor," *Appl. Thermal Eng.*, vol. 50, no. 1, pp. 318–326, Jan. 2013.
[18] W. Soedel, "Introduction to computer simulation of positive displacement type compress," in *Proc. Purdue Compressor Conf.* West Lafayette, IN, USA: Short Course, 1972, pp. 35–42.
[19] J. F. Hamilton, "Extensions of mathematical modeling of positive displacement type compressors," in *Proc. Purdue Compressor Conf.* West Lafayette, IN, USA: Short Course, 1974, pp. 9–25.
[20] R. Prakash and R. Singh, "Mathematical modeling and simulation of reciprocating compressors," in *Proc. Int. Compressor Eng. Conf.*, West Lafayette, IN, USA, 1974, pp. 125–143.
[21] M. L. Todescat, F. Fagotti, and A. T. Prata, "Thermal energy analysis in reciprocating hermetic compressors," in *Proc. Int. Compressor Eng. Conf.* West Lafayette, IN, USA: Purdue Univ., 1992, pp. 1419–1428.
[22] A. Giovanni Longo and R. Caracciolo, "Unsteady state analysis of a hermetic reciprocating compressor: Heat transfer inside the cylinder and valve dynamics," in *Proc. Int. Compressor Eng. Conf.* West Lafayette, IN, USA: Purdue Univ., 2002, p. C4-4.
[23] J. Wang, Q. Li, and J. Li, "Investigation of gas compression process for reciprocating compressor," *Fluid Mach.*, vol. 36, no. 1, pp. 22–25,2008.
[24] M. Farzaneh-Gord, A. Niazmand, M. Deymi-Dashtebayaz, and H. R. Rahbari, "Thermodynamic analysis of natural gas reciprocating compressors based on real and ideal gas models," *Int. J. Refrig.*, vol. 56, pp. 186–197, Aug. 2015.
[25] A. Niazmand, M. Farzaneh-Gord, and M. Deymi-Dashtebayaz, "Exergy analysis and entropy generation of a reciprocating compressor applied in CNG stations carried out on the basis models of ideal and real gas," *Appl. Thermal Eng.*, vol. 124, pp. 1279–1291, Sep. 2017.
[26] Z. Hongfei, *Thermodynamics and the Basis of Heat Transfer*. Shanghai, China: Science Press, 2017.
[27] D. McCloy and H. Martin, *Control of Fluid Power: Analysis and Design*, 2nd ed. Chichester, U.K.: Ellis Horwood, 1980.
[28] N. Govindan, V. Jayaraman, R. Venkatasamy, and M. Ramasamy, "Mathematical modeling and simulation of a reed valve reciprocating air compressor," *Thermal Sci.*, vol. 13, no. 3, pp. 47–58, 2009.
[29] W. Yezheng, *Mathematical Model and Application of Reciprocating Compressor*. Xi'an, China: Xi'an Jiaotong Univ. Press,1986.
[30] Y. Cengel, *Heat Transfer: A Practical Approach*. Boston, MA, USA: McGraw-Hill, 1998.
[31] D. Roskosch, V. Venzik, and B. Atakan, "Thermodynamic model for reciprocating compressors with the focus on fluid dependent efficiencies," *Int. J. Refrig.*, vol. 84, pp. 104–116, Dec. 2017.

XIAOHUI GAO received the Ph.D. degree in mechanical engineering from Beihang University, Beijing, China, in 2016. From 2017 to 2019, he had done the postdoctoral research at Beihang University. He has been working as an Assistant Professor with the Department of Mechatronic, Beihang University. His research interests include compressor, hydraulic servo control, smart material actuator, and nonlinear control.

YONGGUANG LIU received the Ph.D. degree in mechanical engineering from the Harbin University of Technology, Harbin, China, in 1994. From 1999 to 2002, he had done the postdoctoral research at Tsinghua University. He has been working as an Associate Professor with the Department of Mechatronic, Beihang University. His research interests include compressor, hydraulic servo control, industrial robots, network control, and nonlinear active vibration control.